JOURNAL OF THE PHYSICAL SOCIETY OF JAPAN Vol. 13, No. 8, AUGUST, 1958

Absorption Spectra of Cr^{3+} in Al_2O_3

Part B. Experimental Studies of the Zeeman Effect and Other Properties of the Line Spectra

By Satoru SUGANO

Department of Physics, Faculty of Science
University of Tokyo, Tokyo

and Ikuji TSUJIKAWA

Research Institute for Iron, Steel and Other Metals, Tohoku University, Sendai

(Received April 5, 1958)

The absorption intensities, widths and wave-numbers of R_1, R_2 and B_1 B_2 lines of Cr^{3+} in ruby for the polarized light $E \perp C_3$ and $E // C_3$ are experimentally studied at 20°K and 4.2°K. Zeeman effect is also studied, using a magnetic field $H_0 = 24{,}000\,\phi$, for both R and B lines. The Zeeman effect has not been observed yet for the B lines, while Lehmann has already observed the Zeeman effect for R lines. In our results of R lines, the quantitative aspects of Lehmann's experiment are improved. The comparison is made with the theoretical results given in Part A and it is shown that nice agreements can be obtained when suitable assignments of the spectra are adopted and when fairly large g-shifts of the excited states are introduced.

§ 1. Introduction

Among the bound transition metal ions which show extremely narrow absorption spectra e.g., Cr^{3+}, Mn^{2+}, Co^{2+} and Ni^{2+} in complex salts or Cr^{3+} impurity in oxide crystals, ruby Cr^{3+}: Al_2O_3 seems to be the most appropriate material, as explained in § 1 of the first paper of this series, to start the studies of these line spectra.

The general behaviour of the many absorption and emission spectra of ruby has been revealed by the original work of Deutschbein.[1] From this we know that, among the numerous observed spectra, R_1, R_2 lines in the red region and B_1, B_2 in the blue region are conspicuously strong and sharp. Especially on R_1, R_2 lines, Lehmann[2] has examined their optical Zeeman effect at 83°K and

has obtained the Zeeman patterns that depend on the directions of the electric vector E of the incident light and of a magnetic field H_0 relative to the crystal axis C_3.

On the other hand, the Zeeman splitting of the ground level of ruby has been recently measured by the paramagnetic resonance method[3] and its splitting factors have been precisely determined. This enables us to expect that the optical Zeeman pattern must contain some Zeeman components of the ground state whose separations are already known, when the optical Zeeman pattern consists of more than two components and the excited state concerned with is considered to be a Kramers doublet. This is because that, in this case, at least two of such Zeeman components must correspond to the transitions from the different Zeeman levels of the ground state to the same Zeeman level of the excited state.

In Lehmann's Zeeman patterns, however, it is impossible to find out the Zeeman components whose separation corresponds to any separation among the Zeeman levels of the ground state. The theoretical investigation given in the first paper also showed that though the qualitative aspects of Lehmann's results could be reasonably explained, the splitting factors he had measured were far from the theoretical expectation. In such a situation, it was felt necessary to repeat the studies of the Zeeman effect of these line spectra at experimentally better condition.*

In this paper the Zeeman effects of R_1, R_2 (§ 4) and B_1, B_2 (§ 5) lines are studied at 20°K and 4.2°K. The Zeeman patterns of B_1, B_2 have not been observed yet. To determine the magnitudes of Zeeman splittings precisely, we have tried to make the spectral widths narrow by using ruby of low Cr^{3+} concentration as well as by performing the experiment at very low temperatures. The concentration dependence of the spectral width and position (§ 3) has been found in the preliminary course of our work.

Besides the Zeeman effect, it will also be useful for the spectral assignments to examine the change of absorption wave-numbers and intensities (anisotropy) of these spectra when we use polarized light of $E \perp C_3$ and $E // C_3$. The results of such examinations at 20°K and 4.2°K (§ 3) will also serve for extending Paetzold's work[4] which has aimed at the problem of the interaction between chromophoric electrons and lattice by examining the temperature dependence of the absorption wave-numbers and the widths of these spectra at temperatures higher than 80°K.

§ 2. The Experimental Methods

The samples used in our experiments are synthetic rubies of 4 mm thickness (sample A) and of 1 mm thickness (sample B). The crystal axes are determined by X-ray and we cut the sample to make the principal axis C_3 (optic axis) to lie in the plain, perpendicularly to which the incident light is passed. The result of chemical analysis shows that samples A and B contain 0.28 and 2.56 weight percent Cr_2O_3 respectively.

In our spectroscopic studies, a grating spectrograph in Eagle mounting with dispersion 2.5 Å/mm in the first order has been used. The light source is a 60–W Zircon-lamp and the diffracted beam is detected by photographic methods. The comparison spectra are supplied by Ne-lamp (6929.468Å, 7032.413 Å lines) or Cd-lamp (4679.156 Å, 4799.-918Å lines) corresponding to the case of determining R_1, R_2 or B_1, B_2 absorption wave-lengths. In the determination of the latter, however, it is sometimes more convenient to utilize the emission lines of the light source (the arc lines of Zr, 4739.478Å, 4772.312Å) as the comparison spectra.

To get the light beams polarized perpendicularly to each other, Wollaston's prism is placed in front of the slit and through the separated parts of the slit both polarized beams are passed simultaneously. Thus in every exposure we can get two kinds of spectral photograph corresponding to the polarized beams $E \perp C_3$ and $E // C_3$. In this case, the astigmatism of the concave grating is eliminated by the cylindrical lens suitably placed in front of the photographic plate.

Further in our absorption measurements of R_1 and R_2, we have inserted, between the light source and the sample, the red filter in order to cut the light of shorter wave-length which lies in the region of the broad absorp-

* Prof. G. H. Dieke of the Johns Hopkins University has kindly informed us that Zeeman experiment on ruby has also been completed in his laboratory but the results are not published yet.

tion bands U and Y located at ~5500Å and ~4000Å; Ruby shows relatively strong emission at the same positions as those of R_1, R_2 when it is excited by visible light in the region of U and Y and so in the absorption measurements we must suppress the undesired emission parts of R_1, R_2 lines by exclusion of such excitation light.

To keep a sample at low temperatures, it is immersed in liquid helium or liquid hydrogen contained in a Dewar vessel. The magnitude of the applied magnetic field to study the Zeeman effects is 24,000 ϕ.

§ 3. Properties of the Line Spectra in Absence of a Magnetic Field

(a) *The optical anisotropies*: Though no quantitative measurement of the absorption intensities has been attempted, the optical anisotropies observed in R_1, R_2 and B_1, B_2 absorption lines are remarkable and so they are schematically described in Fig. 1. The

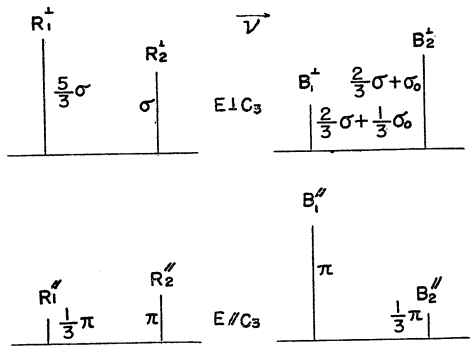

Fig. 1. The optical anisotropies observed in R_1, R_2 and B_1, B_2 absorption lines. Only the relative intensities are schematically represented for R's and B's spectra. The most intense lines $R_1^{\perp}$ and $B_1^{//}$ in each group are normalized.

relation between the intensities of R_1 and R_2 is inverted when the polarization of the incident light is changed. The same situation also occurs in B_1, B_2, though the relation between the intensities of B_1 and B_2 is just contrary to the case of R_1 and R_2 for each polarization.

The qualitative aspects of these anisotropies are not changed when temperature or concentration of Cr^{3+} is varied.

(b) *The spectral widths*: A tremendously large difference is observed between the spectral widths of the relatively dilute sample A and highly concentrated sample B. In sample A, the spectral widths are very narrow and their approximate values are as follows;*

$R_1^{\perp}$	$R_2^{\perp}$	$R_1^{//}$	$R_2^{//}$	
0.7,	0.6,	0.6,	0.6,	(cm^{-1})
$B_1^{\perp}$	$B_2^{\perp}$	$B_1^{//}$	$B_2^{//}$	
1.9,	2.6,	1.9,	2.6,	

No noticeable difference is observed among the spectral widths observed at 86°K, 20°K and 4.2°K for R lines and between those measured at 20°K and 4.2°K for B lines. In sample B, the widths of R_1, R_2 are approximately 3 cm^{-1} and those of B_1, B_2 8 cm^{-1} which are about four times larger than those observed in sample A (also see Fig. 2).

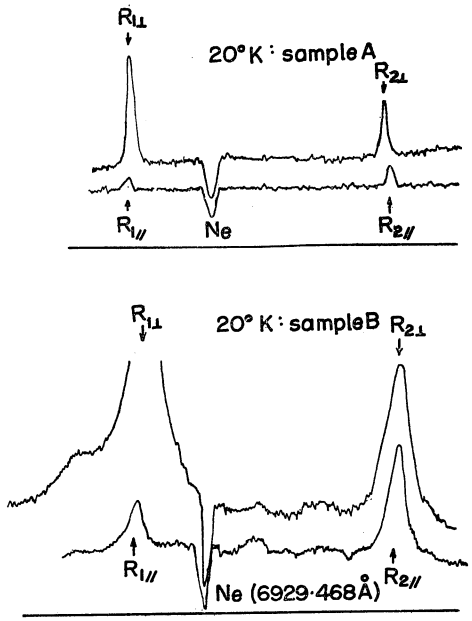

Fig. 2. The microphotometer traces of R_1 and R_2 spectra of samples A and B observed at 20°K.

The spectral widths in sample A are such that in R_1, R_2 lines the widths of $R_1^{\perp}$ is a little larger than the other components and in B_1, B_2 lines the widths of $B_1^{\perp}$ and $B_1^{//}$ are clearly smaller than those of $B_2^{\perp}$, $B_2^{//}$.

(c) *The absorption wave-numbers*: The absorption wave-lengths of R_1, R_2 and B_1, B_2 absorption lines for the polarized lights ($E\perp$

* Throughout this paper, superscripts $\perp$ and // indicate the direction of E and subscripts $\perp$ and // indicate that of H_0 relative to the optic axis C_3.

Table I. R_1, R_2 absorption wave-lengths λ and wave-numbers ν for the polarized light at low temperatures.

Temp.	Polariz.	Spect.	Sample A (dil.)		Sample B (conc.)	
			λ(Å)	ν(cm^{-1})	λ(Å)	ν(cm^{-1})
4.2°K	$E\perp C_3$	R_1	6933.93	14417.87	6933.0	14419.8
		R_2	19.98	46.93	18.8	49.4
	$E//C_3$	R_1	34.03	17.63	33.0	19.8
		R_2	19.83	47.24	18.8	49.4
20°K	$E\perp C_3$	R_1	6933.90	14417.93	6933.0	14419.8
		R_2	19.95	46.99	18.8	49.4
	$E//C_3$	R_1	33.93	17.86	33.0	19.8
		R_2	19.75	47.41	18.8	49.4
86°K	$E\perp C_3$	R_1	6934.01	14417.70	6933.2	14419.4
		R_2	20.06	46.76	19.0	49.0
	$E//C_3$	R_1	34.01	17.70	33.2	19.4
		R_2	19.91	47.08	19.0	49.0
Exp. error			±0.02	±0.04	±0.1	±0.2

Table II. B_1, B_2 absorption wave-lengths λ and wave-numbers ν for the polarized light at low temperatures.

Temp.	Polariz.	Spect.	Sample A (dil.)		Sample B (conc).	
			λ(Å)	ν(cm^{-1})	λ(Å)	ν(cm^{-1})
4.2°K	$E\perp C_3$	B_1	4762.24	20992.7	4762.3	20992
		B_2	45.27	21067.7	45.3	21068
	$E//C_3$	B_1	62.18	20992.9	62.3	20992
		B_2	45.35	21067.4	45.3	21068
20°K°	$E\perp C_3$	B_1	4762.26	20992.6	4762.2	20993
		B_2	45.27	21067.7	45.6	21066
	$E//C_3$	B_1	62.18	20992.9	62.2	20993
		B_2	45.37	21067.3	45.6	21066
Exp. error			±0.03	±0.1	±0.2	±1

Table III. The separations of R_1 and R_2 absorption spectra and their polarization-shifts $\nu^{\perp}-\nu^{//}$. (cm^{-1})

	Sample A			Sample B		
	4.2°K	20°K	86°K	4.2°K	20°K	86°K
$\nu(R_2^{\perp})-\nu(R_1^{\perp})$	29.06	29.06	29.06	29.6	29.6	29.6
$\nu(R_2//)-\nu(R_1//)$	29.61	29.55	20.38			
$\nu(R_1^{\perp})-\nu(R_1//)$	0.24	0.07	0.00	——	——	——
$\nu(R_2^{\perp})-\nu(R_2//)$	−0.31	−0.42	−0.32	——	——	——

C_3 and $E//C_3$) have been measured precisely as possible and they are given in Tables I and II. The experimental error given in the tables is caused mainly by the difficulty of determining the position of an absorption peak because of the finite spreading of the spectrum.

The most remarkable fact found in such measurements is that the absorption position of the spectrum slightly shifts when the polarization of the incident light is changed (called hereafter polarization-shift). The directions and the magnitudes of these shifts are shown in the last two rows of Tables III and IV, together with the observed separations between R_1 and R_2 and those between B_1 and B_2. These separations and polarization-shifts seem independent of the change of temperature except for the separation $\nu(R_2//) - \nu(R_1//)$ and the shift $\nu(R_1{}^{\perp}) - \nu(R_1//)$.

Table IV. The separations of B_1 and B_2 absorption spectra and their polarization-shifts $\nu^{\perp} - \nu//$. (cm^{-1})

	Sample A		Sample B	
	4.2°K	20°K	4.2°K	20°K
$\nu(B_2{}^{\perp}) - \nu(B_1{}^{\perp})$	75.0	75.1	76	76
$\nu(B_2//) - \nu(B_1//)$	74.5	74.4		
$\nu(B_1{}^{\perp}) - \nu(B_1//)$	−0.2	−0.3	—	—
$\nu(B_2{}^{\perp}) - \nu(B_2//)$	0.3	0.4	—	—

The temperature dependence of the absorption wave-numbers of R_1 and R_2 is illustrated in Fig. 3. When the temperature is increased from 4.2°K to 20°K, these spectra shift towards the shorter wave-length side (blue-shift), while they show a red-shift at high temperatures. The shifts thus found at very low temperatures are, however, so small (the order of these magnitudes is different from that observed at high temperatures) that they cannot be observed in case of B lines, being within the experimental error.

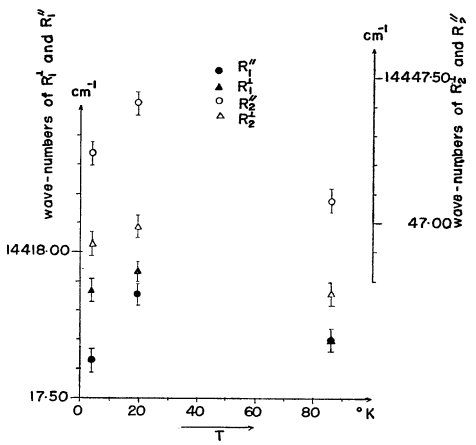

Fig. 3. The temperature dependences of the absorption wave-numbers of $R_1^{\perp}$, $R_1//$, $R_2^{\perp}$ and $R_2//$ (sample A).

In sample B, the absorption positions of R_1 and R_2 lines seem to be shifted towards the shorter wave-length side beyond the experimental error (Table I) in comparison with those measured in sample A, while these concentration-shifts are not clearly observed in B_1, B_2 lines.

(d) *Discussions*: The observation of optical anisotropies provides us with a very useful information for the spectral assignment, especially in case the spectral width is broad and experimental studies of the Zeeman effect are impossible to be made. Theoretically the absorption intensities of the line spectra in our case are supplied from those of the absorption bands by interplay of spin-orbit interaction, i.e., the intensity of R lines is supplied from U band and that of B lines mainly from Y and partly from U. Thus the optical anisotropies of these lines are determined both by the anisotropies of the absorption bands and by the strengths of spin-orbit interactions. In Fig. 1, the results of the theoretical estimates of optical intensities (Part A § 5 (b)) are also given under the presumption that the spectral assignment has been made as follows,*

$$\left.\begin{array}{ll} R_1: & {}^4A_2 \rightarrow \overline{E} \\ B_2: & \rightarrow 2\overline{A} \end{array}\right\} {}^2E$$

$$\left.\begin{array}{ll} B_1: & {}^4A_2 \rightarrow 2\overline{A} \\ B_2: & \rightarrow \overline{E}_a \end{array}\right\} {}^2F_2 .$$

We see that the qualitative features of the observed relative intensities for the fixed polarized light are reasonably explained by the theory, though the theory does not explain the intensity ratio between parallel and perpendicular component of a spectrum. Our experimental results recommend the following

* On the meaning of the notations, see Part A. Throughout this paper, we use the notations already used in Part A without explaining their meaning.

approximate relations among the theoretically introduced parameters; $\sigma \sim 2\pi$ (for ^2E), $\sigma_0 \sim 2\sigma$ and $\pi \sim 3\sigma$ (for $^2F_2$).

The problem of the observed separations of R_1 and R_2 and of B_1 and B_2 lines has been already discussed in Part A. The separation is determined mainly by the magnitudes of the trigonal field and the spin-orbit interaction. The remarkable constancy of the observed separations (except $\nu(R_2^{//})-\nu(R_1^{///})$) at low temperatures will indicate that little change of the crystal parameters occurs at these temperatures. The exceptional case $\nu(R_2^{//})-\nu(R_1^{//})$ is brought about by the anomalous temperature dependence of $R_1^{//}$ spectrum. Although $R_1^{//}$ is the faintest spectrum among R's, its observed anomaly seems to be really the case being beyond the experimental error. This anomaly remains unexplained.

The polarization-shifts can be easily understood if attention is paid both to the selection rule and the initial splitting of the ground state (see Figs. 4 and 5 of Part A). Thus the assignments are also confirmed by observing these polarization-shifts. If the sign of δ is defined positive when the Kramers doublet $M_s=\pm 3/2$ is lower than the doublet $M_s=\pm 1/2$, the theoretically predicted polarization-shifts are as follows under the above-mentioned spectral assignments;*

$$\delta/2 < \nu(R_1^{\perp})-\nu(R_1^{//}) < \delta\,,$$
$$\nu(R_2^{\perp})-\nu(R_2^{//}) = -\delta\,,$$
$$\nu(B_1^{\perp})-\nu(B_1^{//}) = -\delta\,,$$
$$\delta/2 < \nu(B_2^{\perp})-\nu(B_2^{//}) \lesssim \delta.\ (|\delta| = 0.38\ \mathrm{cm^{-1}})$$

The experimental results given in Tables III and IV (except $\nu(R_1^{\perp})-\nu(R_1^{//})$) satisfy these relations within the limit of the experimental error when the sign of δ is assumed positive. The exceptional case of $\nu(R_1^{\perp})-\nu(R_1^{//})$ is because of the queer behaviour of $R_1^{//}$ spectrum which has been already pointed out. Since the polarization-shift of R_2 spectrum is measurable with rather high precision, its measurement is one of the ways to determine optically the natural splitting δ. The value of δ thus determined from the polarization-shift of R_2 is $\delta = 0.36 \pm 0.03\ \mathrm{cm^{-1}}$ which agrees well with the result of the paramagnetic resonance experiments, $|\delta| = 0.38\ \mathrm{cm^{-1}}$.[3] Such an optical method is superior to the paramagnetic resonance method only in determining the sign of δ.

The problems of the spectral widths and the temperature-shifts will not be discussed in detail in this paper. The slight broadness of $R_1^{\perp}$ compared with the other components of R_1 and R_2 can be understood since theoretically $R_1^{\perp}$ spectrum is the superposition of two lines separated by δ while the others are singlets. To interpret the difference between the widths of B_1 and B_2 lines, however, it is necessary to take other effects into consideration. The curious temperature-shifts of R lines observed at very low temperatures show that Paetzold and Krömer's experimental formula[5] $\nu = \alpha + \beta(T/\Theta)^2$ at $T \ll \Theta$ (Θ: Debye temperature) is not good for R lines at these temperatures.

The observed concentration-broading and concentration-shift seem to offer very interesting problems, but to discuss such problems it will be necessary to make further experiments.

§ 4. Zeeman Effects of R_1 and R_2 Absorption Lines

The Zeeman patterns of R_1, R_2 absorption lines of sample A obtained at 20°K and 4.2°K in the four cases, $H_0//C_3$ $E\perp C_3$, $H_0//C_2$ $E//C_3$, $H_0\perp C_3$ $E\perp C_3$, and $H_0\perp C_3$ $E//C_3$ are illustrated in Figs. 4 and 5 together with the diagrams of transitions.

The observed splitting factors g's and the central wave-numbers ν^0's of these patterns are listed in Table V. Among these Zeeman patterns, those of R_1 ($H_0//C_3$ $E//C_3$) and of R_1, R_2 ($H_0\perp C_3$ $E//C_3$) are too faint to make direct measurements of the original plates precisely. Therefore, suitably reprinted plates with high contrast have been used for the measurements.

In the reprinted plates, it is found that, though the relative positions of absorption

* In the following relations, inequalities occur because $R_1^{\perp}$ and $B_2^{\perp}$ are expected to be unresolved doublets separated by δ (Figs. 4 and 5, Part A) and the observed peak of an unresolved doublet is considered to be located between the middle of the unresolved doublet and the stronger component of the doublet. The observed peak will be just at the middle of the unresolved two components when their intensities are same. In the following discussions, inequalities always appear in such cases.

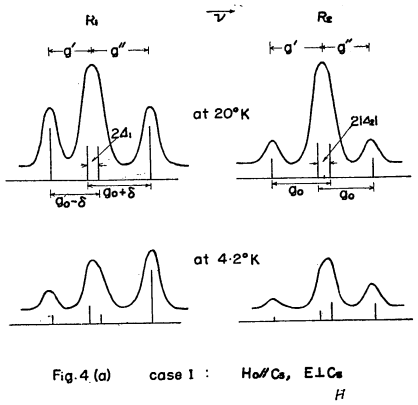

Fig. 4 (a) case I : $H_0 /\!/ C_3$, $E \perp C_3$

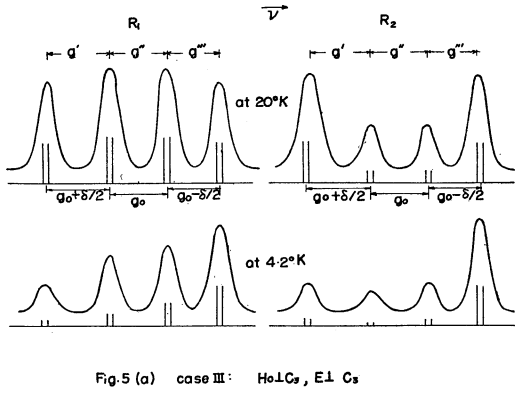

Fig. 5 (a) case III : $H_0 \perp C_3$, $E \perp C_3$

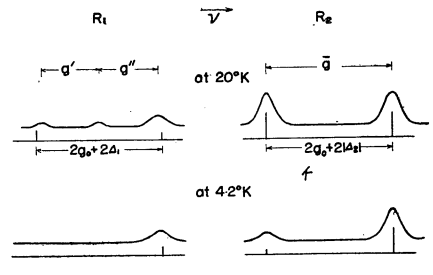

Fig. 4 (b) case II : $H_0 /\!/ C_3$, $E /\!/ C_3$

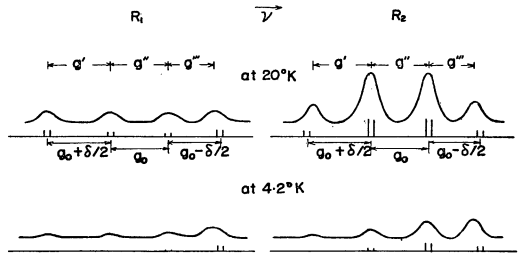

Fig. 5 (b) case IV : $H_0 \perp C_3$, $E /\!/ C_3$

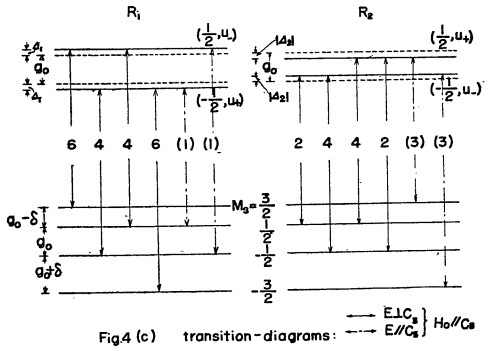

Fig. 4 (c) transition-diagrams: $E \perp C_3$, $E /\!/ C_3$ } $H_0 /\!/ C_3$

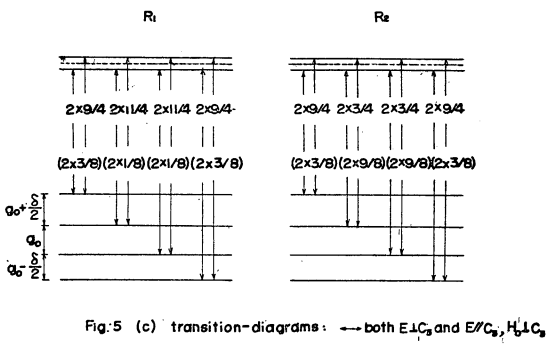

Fig. 5 (c) transition-diagrams: both $E \perp C_3$ and $E /\!/ C_3$, $H_0 \perp C_3$

Fig. 4, 5. (a), (b): The observed Zeeman patterns (full curve) and the patterns (vertical lines) derived from the transition-diagrams (c). The intensities and the shapes of the observed patterns are only qualitatively illustrated. In the patterns (vertical lines) of 4.2°K, difference in electron population of the Zeeman levels of the ground state is taken into account. (c): The numbers in brackets indicate the transition probabilities when $E||C_3$ and the others (without brackets) are those when $E \perp C_3$. In the calculation of the transition probabilities, the empirical relation $\sigma \sim 2\pi$ is used and π is put equal to 1.

lines are represented fairly well, the distance between an emission (comparison spectrum) and an absorption line is sometimes slightly changed from that measured on the original plate. Thus in order to avoid the confusion such unreliable measurements on the absolute positions of the absorption may create, the central wave-numbers ν^0's of these faint patterns are not tabulated. In Table VI the quantities derived from Table V which are useful in the following discussions are also given.

All the qualitative features of the Zeeman patterns obtained at 20°K are in agreement with those obtained by Lehmann at 83°K, but the quantitative features of our patterns

Table V. The observed splitting factors (in βH_0 unit) and the central wave-numbers $\nu^0(\mathrm{cm}^{-1})$ of R_1, R_2 Zeeman patterns. The central wave-number ν^0 is defined as the wave-number of the central Zeeman component when three Zeeman components appear, and is defined as the wave-number in the middle of the inner two components when four components appear. On the notation of g's, see Fig. 4.

$H_0=24{,}000\,\phi$ $\beta H_0=1.12\,\mathrm{cm}^{-1}$			20°K		4.2°K		Exp. error
			R_1	R_2	R_1	R_2	
$H_0 // C_3$	$E \perp C_3$	g'	1.46	1.80	1.45	1.92	±0.07
		g''	2.04	1.64	2.12	1.53	
		ν^0	14417.51	14446.85	14417.66	14447.16	±0.04
	$E // C_3$	g'	2.1		——		±0.1
		$\bar{g}$		4.38		4.42	±0.07
		g''	2.0		——		±0.1
		ν^0	——	14447.31	——	14447.29	±0.04
$H_0 \perp C_3$	$E \perp C_3$	g'	2.15	2.09	2.13	2.12	±0.07
		g''	1.96	1.92	1.98	2.03	
		g'''	1.80	1.73	1.80	1.79	
		ν^0	14417.89	14417.21	14417.96	14447.31	±0.04
	$E // C_3$	g'	2.2	2.0	2.1	2.1	±0.1
		g''	2.0	2.0	1.9	2.0	
		g'''	1.6	1.6	1.9	1.7	

are entirely different from those of Lehmann's.

To simplify the description, we assume from the beginning the spectral assignments given in § 3 (d) which are established most definitely from the observed Zeeman patterns.

Case I. $H_0 // C_3$ and $E \perp C_3$ (Fig. 4 (a)):

The observed splitting factors of the Zeeman patterns in this case are far smaller than those theoretically expected, even though they are increased compared with those of Lehmann's.

The only way to fulfil the previously given proper requirement that the Zeeman pattern in this case must contain some of the Zeeman components of the ground state is to introduce the g-shifts of the excited states assuming the central component to be the unresolved doublet. In fact the central component seems broader than the side components. That this is due to the superposition of two lines can be made clear by observing its apparent shift relative to the side component when the temperature is varied from 20°K to 4.2°K. This is because, if the central component is the superposition of closely located two lines, the decrease of the number of electrons populated in the upper Zeeman levels of the ground states at 4.2°K makes one line of the superposed two central lines weaker than the other. As a result, the apparent peak of the central component shifts to the stronger one while at 20°K it will be almost at the middle of the two.

The quantities $1/2(g_{//}''-g_{//}')$ measured at 20°K and 4.2°K given in the second row of Table VI show such apparent relative shifts of the central component for both R_1 and R_2. Keeping the above-mentioned explanation of the apparent shifts in mind and refering to the theoretically obtained diagram of transitions, we expect the following values for $1/2(g''-g')$;

$$\left.\begin{aligned} 1/2(g_{//}'-g_{//}') &= \delta \text{ for } R_1 \\ &= 0 \text{ for } R_2 \end{aligned}\right\} \text{ at } 20°\mathrm{K}$$

$$\left.\begin{aligned} &> \delta \text{ and } < \delta+|\Delta_1| \text{ for } R_1 \\ &> -|\Delta_2| \text{ and } < 0 \quad \text{for } R_2 \end{aligned}\right\} \text{ at } 4.2°\mathrm{K},$$

where Δ_1 and Δ_2 denote the half g-shifts of the excited states of R_1 and R_2 respectively and their magnitudes will be determined in the following analysis. With the values Δ_1

$=0.22$, $\Delta_2=-0.26$ and $\delta=0.34$ (in βH_0 unit), these relations are held actually in Table VI almost within the limit of experimental error.

The g-shifts of the R_1 and R_2 excited states are determined from

$$1/2(g_{//}'+g_{//}'')=g_0-\Delta_1 \quad \text{for } R_1,$$
$$=g_0+\Delta_2 \quad \text{for } R_2,$$

where g_0 is the g-value of the ground state and is known as 1.98. The sum of the left hand side is made to eliminate the effect of the natural splitting δ of the ground state. From Table VI, we obtain

$$\Delta_1=0.22\ (\pm0.04),\quad \Delta_2=-0.26\ (\pm0.04),$$
$$g_{e//}(R_1)=g_0+2\Delta_1=2.42,$$
$$g_{e//}(R_2)=g_0+2\Delta_2=1.46,$$

where $g_{e//}(R_1)$ and $g_{e//}(R_2)$ are the g-values of the R_1 and R_2 excited states respectively. Looking at these results, we notice at once the following simple relation to exist between $g_{e//}$'s,

Table VI. The useful quantities to confirm the assignments. These are derived from Table I and Table V. $g_{//}$ and $g_{\perp}$ denote the splitting factors in cases of $H_0//C_3$ and $H_0\perp C_3$ respectively. The subscripts of $\nu_{//}^0$ and $\nu_{\perp}^0$ also indicate the direction of a magnetic field. ν_0 is the absorption wave-number in case of no magnetic field.

$E\perp C_3$		R_1	R_2
$\frac{1}{2}(g_{//}'+g_{//}'')$	20°K	$1.75\beta H_0$	$1.72\beta H_0$
	4.2°K	1.78	1.72
$\frac{1}{2}(g_{//}''-g_{//}')$	20°K	0.29	−0.08
	4.2°K	0.33	−0.19
$\nu_{//}^0-\nu_0$	20°K	-0.42cm^{-1}	-0.14cm^{-1}
	4.2°K	−0.21	+0.23
$g_{\perp}''$	20°K	$1.96\beta H_0$	$1.92\beta H_0$
	4.2°K	1.98	2.03
$\frac{1}{2}(g_{\perp}'+g_{\perp}'')$	20°K	1.97	1.91
	4.2°K	1.96	1.95
$g_{\perp}'-g_{\perp}'''$	20°K	0.35	0.36
	4.2°K	0.33	0.33
$\nu_{\perp 0}-\nu_0$	20°K	-0.04cm^{-1}	$+0.23\text{cm}^{-1}$
	4.2°K	+0.09	+0.38
$E//C_3$			
$\nu_{//}^0-\nu_0$	20°K	—	-0.10cm^{-1}
	4.2°K		+0.05

$$g_{e//}(R_1)+g_{e//}(R_2)\fallingdotseq 4,$$

since

$$\Delta_1\fallingdotseq-\Delta_2\ (\neq 0).$$

The explanation of such an interesting relation between the g-shifts of the R_1 and R_2 excited states is given in the first paper.

Case II. $H_0//C_3$ and $E//C_3$ (Fig. 4 (b)):

The $g_{e//}$ (R_2)-shift is more clearly observed in this case in the Zeeman pattern of R_2 where the separation of the two components $\bar{g}$ must be $2g_0-2\Delta_2=4.52$ (±0.07) if the same $g_{e//}(R_2)$-shift as determined from the pattern of $R_2^{\perp}$ in the previous case is used. The observed values of $\bar{g}$'s for the both temperatures (Table VI) agree with this within the limit of experimental error.

The observed Zeeman pattern of $R_1//$ which is the faintest among the patterns of R_1 and R_2 we have obtained, however, does not seem to be explained within our scheme even qualitatively. Against our expectation on this pattern that it consists of two weak components separated by $2g_0+2\Delta_1=4.40$ (±0.07), the observed pattern consists of three components and the separation of the side components is 4.1 (±0.1) even if the central component is disregarded. Our previous short report[6] has erroneously described this Zeeman pattern.

Case III $H_0\perp C_3$ and $E\perp C_3$ (Fig. 5 (a)).

In this case, the Zeeman levels of the ground state are directly represented: The paramagnetic resonance experiment has show that the separation of the four Zeeman levels of the ground state are $g_0-\delta/2$, g_0 and $g_0+\delta/2$. If $g_{\perp}'''$, $g_{\perp}''$ and $g_{\perp}'$ are identified to be $g_0-\delta/2$, g_0 and $g_0+\delta/2$ respectively, the relations,

$$g''=g_0=1.98,\quad 1/2(g'+g'')=g_0,$$
$$g_{\perp}'-g_{\perp}'''=\delta=0.34$$

must hold among the observed $g_{\perp}$'s. Table VI shows that the observed $g_{\perp}$'s actually satisfy these relations within the limit of experimental error. The positive sign of δ is also confirmed in such a comparison. In the Zeeman patterns observed at 4.2°K, the uniformly decreasing inclination of the intensities of the longer wave-length side components which is due to the decrease in electron population of the upper Zeeman levels of the ground state at 4.2°K is consis-

tent with the above-mentioned identification of the observed $g_\perp$'s. In this case, the g-shifts $\Delta g_{e\perp}$'s, i.e., deviations of the g-values of the excited states from zero, will split each of the four Zeeman components into two lines separated by $\Delta g_{e\perp}$, but, if $\Delta g_{e\perp}$'s are smaller than the spectral width, these closely located two lines cannot be resolved and the apparent position of such a superposed component will not be changed from the case of $\Delta g_{e\perp}=0$. In addition to this situation, since the superposed two lines correspond to the transitions from the same Zeeman level of the ground state, the apparent temperature-variations of the splitting factors similar to those previously explained in case of $H_0 // C_3$ and $E\perp C_3$ are not expected. In Fig. 5, the finite g-shifts of the both R_1 and R_2 excited states are assumed although they cannot be determined from the observed patterns.

Case IV $H_0\perp C_3$ and $E // C_3$ (Fig. 5 (b)):

An accurate measurement of the splittings is impossible in this case because the intensities are weak. It may be said, however, from Table V that no noticeable difference of the splittings is observed between case III and case IV, which is resonable from the theoretical point of view. The relative intensities of the components, which differ from those observed in case III show a nice agreement between experiment and theory.

A remaining quantity to be discussed is the central wave-number ν^0 of the Zeeman pattern whose definition is given in the footnote of Table V. According to the diagram of transitions, the difference between ν^0 and ν_0 observed in case of no magnetic field, $\Delta\nu=\nu^0-\nu_0$, must satisfy the following relations; when $H_0 // C_3$ and $E\perp C_3$

$$0 > \Delta\nu(20°\mathrm{K}) > \delta \quad (=0.38\ \mathrm{cm}^{-1})$$
$$\Delta\nu(20°\mathrm{K}) > \Delta\nu(4.2°\mathrm{K}) > \Delta\nu(20°\mathrm{K})-|\Delta_1| \quad (|\Delta_1|=0.25\ \mathrm{cm}^{-1})$$
for R_1;
$$\Delta\nu(20°\mathrm{K})=0$$
$$|\Delta_2| > \Delta\nu(4.2°\mathrm{K}) > 0 \quad (|\Delta_2|=0.29\ \mathrm{cm}^{-1})$$
for R_2;

when $H_0 // C_3$ and $E // C_3$

$$\Delta\nu(20°\mathrm{K},\ 4.2°\mathrm{K})=0 \quad \text{for } R_2;$$

when $H_0\perp C_3$ and $E\perp C_3$

$$0 > \Delta\nu(20°\mathrm{K},\ 4.2°\mathrm{K}) > 3\delta/4-\delta \quad (=0.10\ \mathrm{cm}^{-1}) \text{ for } R_1;$$
$$\Delta\nu(20°\mathrm{K},\ 4.2°\mathrm{K})=3\delta/4 \quad (=0.28\ \mathrm{cm}^{-1}) \text{ for } R_2;$$

The observed $\Delta\nu$'s given in Table VI seem to deviate from these beyond the limit of experimental error. All deviations are systematic in such a way that they are negative at 20°K and positive at 4.2°K.

§ 5. Zeeman Effect of B_1 and B_2 Absorption Lines

The observed Zeeman patterns of B_1, B_2 absorption lines are illustrated in Fig. 6 and Fig. 7 together with the diagram of transitions. The spectral widths of B_1 and B_2 lines are about three times broader than those of R_1 and R_2, but they are still smaller or comparative to the Zeeman energies. Therefore we have obtained the Zeeman patterns, although not so clear as the case of R lines, which depend on the directions of H_0 and E relative to the crystal axis C_3. Thus, together with the theoretical considerations given in the first paper, it is possible to establish definite assignments of B lines by using the observed patterns. For example, a possibility that one of these spectra may be identified to the transition ${}^4A_2 \rightarrow \bar{E}_b({}^2F_2)$ can be easily excluded by the fact that the theoretically predicted Zeeman patterns corresponding to it (Fig. 5, Part A) consists of an unsplit component when $H_0 // C_3$ and $E // C_3$ (it consists of two components separated by $2\beta H_0$ when $H_0 // C_3$ and $E\perp C_3$). We cannot find such a pattern in the observed Zeeman patterns.

In the following discussions, we will assume from the beginning the assignments given in § 3 (d), in the same way as we have done in § 4, and will show to what degree such assignments are convincing.

To observe the faint and diffuse Zeeman patterns, it was necessary to use the suitably reprinted plates instead of using the original ones.

Case I $H_0 // C_3$ and $E\perp C_3$ (Fig. 6 (a)):

The Zeeman splitting can be observed rather clearly in $B_1^\perp$ spectrum at 20°K while only vaguely in $B_2^\perp$ at 20°K. In the diagrams of transitions, the finite $g_{e//}$-shift (from zero), Δ_1', of the B_1 excited state and also the finite

$g_{e//}$-shift (from 4), Δ_2', of the B_2 excited state are assumed. Comparing the experimental patterns with those expected from such transition diagrams, a rather good agreement can be obtained if Δ_2' satisfies the relation $g_0-2\Delta_2' \sim g_{obs}(B_2)=2.4+0.5$ (so $\Delta_2' \sim 0.2\pm 0.25$) and if $2\Delta_1'$ is small compared with g_0. Even when Δ_1' differs from zero, $g_{obs}(B_1)=2.1\pm0.2$ is reasonable considering the fact that at 20°K the observed position of the apparent peak will be almost at the middle of the closely located two lines since their intensities become equal when we assume the relation $\sigma_0 \sim 2\sigma$. The necessity that Δ_1' ($\neq 0$) must be introduced will be seen in the analysis of Case II.

Case II $H_0//C_3$ and $E//C_3$ (Fig. 6 (b)):

Among all the observed Zeeman patterns of B_1 and B_2, the Zeeman pattern of $B_1//$ at 20°K in this case is most clear. Thus the most definite conclusion can be derived from

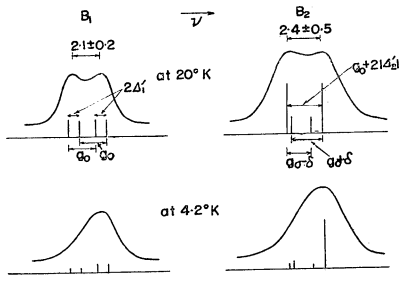

Fig.6 (a) case I : $H_0 // C_3$, $E \perp C_3$

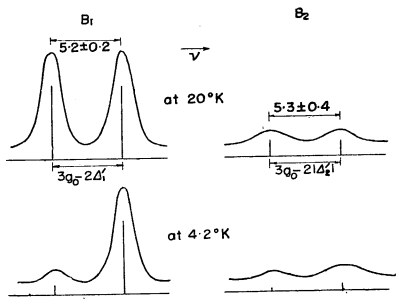

Fig.6 (b) case II : $H_0 // C_3$, $E // C_3$

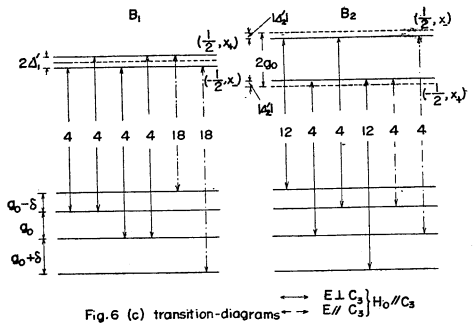

Fig.6 (c) transition-diagrams ⟷ $E \perp C_3$ ⟶ $E // C_3$ } $H_0 // C_3$

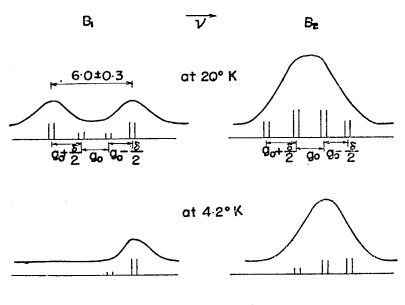

Fig.7 (a) case III : $H_0 \perp C_3$, $E \perp C_3$

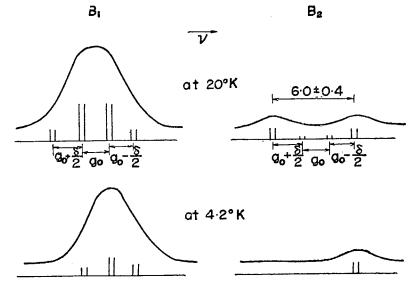

Fig.7 (b) case IV : $H_0 \perp C_3$, $E // C_3$

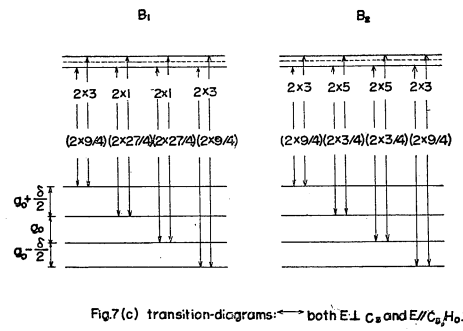

Fig.7 (c) transition-diagrams: ⟷ both $E \perp C_3$ and $E // C_3$, $H_0 \perp C_3$

Figs. 6, 7. (a), (b): The observed Zeeman patterns (full curve) and the patterns (vertical lines) derived from the transition-diagrams (c). The intensities and the shapes of the observed patterns are only qualitatively illustrated. The observed splitting factors are also given in βH_0 unit. In the patterns (vertical) of 4.2°K, difference of the electron population of the Zeeman levels of the ground state is taken into account. (c): The numbers in brackets indicate the transition probabilities when $E||C_3$ and the others (without brackets) are those when $E \perp C_3$. In the calculation of the transition probabilities, the empirical relations $\sigma^\circ \sim 2\sigma$ and $\pi \sim 3\sigma$ are used and σ is put equal to 12.

this pattern. A nice agreement can be obtained between theory and experiment also in this case, when Δ_1' and Δ_2' satisfy the following relations,

$$3g_0-2\Delta_1'=g_{\mathrm{obs}}(B_1)=5.2\pm0.2$$
$$3g_0+2\Delta_2'=g_{\mathrm{obs}}(B_2)=5.3\pm0.4\,.$$

From these relations we obtain

$$\Delta_1'=0.4\pm0.1$$

and

$$\Delta_2'=-(0.3\pm0.2)$$

the latter of which is consistent with the value of Δ_2' ($\Delta_2'\sim0.2\pm0.25$) obtained in case I.

The g-shifts Δ_1' and Δ_2' seem to satisfy the relation $\Delta_1'+\Delta_2'\fallingdotseq0$, and the theoretical examination of such g-shifts (§ 6 (e), Part A) shows that they are directly due to the reduction of the orbital angular momentum of f_2-electrons in the crystal.

Case III $H_0\perp C_3$ and $E\perp C_3$ (Fig. 7 (a)):

The observed patterns seem to be the envelopes of the unresolved Zeeman components. The reasonable interpretation of these patterns can be made in such a way that the observed two peaks of B_1 correspond to the stronger two side components and the pattern of B_2 is determined mainly by the inner two components which are stranger than the side components in this spectrum. The reason why none of the split structures is seen in this case (also in case IV) while they are represented in case I even though slightly in B_2, may be due to the relatively large g-shifts (from zero) of the excited states. Thus in the transition-diagram of Fig. 7 the finite g-shifts of the excited states are assumed though their magnitudes cannot be determined from our Zeeman patterns. The reasonable splitting $g_{\mathrm{obs}}(B_1)=6.0\pm0.3$ of B_1 will not be affected by introducing such g-shifts.

Slight blue-shift of the apparent peak and narrowing of the apparent width of the unresolved Zeeman pattern $B_2^{\perp}$ at 4.2°K compared to the Zeeman pattern observed at 20°K (the situation is also the same about the Zeeman pattern $B_1^{//}$ in case IV) clearly show that the observed broad pattern is the envelope of the Zeeman components.

Case IV $H_0\perp C_3$ and $E//C_3$ (Fig. 7 (b)):

In the same way as explained in case III, the patterns obtained in this case can also be explained reasonably.

Acknowledgements

We should like to express our sincere thanks to Prof. E. Kanda of Tohoku University, Prof. Z. Koana and Prof. G. Kuwabara of the University of Tokyo for their continual encouragements and advices through the course of this work. We are greatly indebted to Dr. T. Imai and Mr. S. Togashi of Nippon Denkō Laboratories for their kindness of preparing the samples which are well examined chemically, and to Prof. R. Sadanaga and Dr. Y. Iitaka of Mineralogy Department of Tokyo University for their kindness of performing X-ray determination of the crystal axis and cutting. Miss K. Shimada was kind enough to prepare the suitably reprinted plates for the detection of some feeble and diffuse Zeeman patterns.

References

1) O. Deutschbein: Ann. d. Phys. [5] **14** (1932) 712, 729; Ann. d. Phys. [5] **20** (1934) 828.
2) H. Lehmann: Ann. d. Phys. [5] **19** (1934) 99.
3) A. A. Manenkov and A. M. Prokhorov: J.E.T.P. **28** (1955) 762.
M. M. Zaripov and Iu. Ia. Shamonin: J.E.T.P. **30** (1956) 291.
J. E. Geusic: Phys. Rev. **102** (1956) 1252.
4) K. H. Paetzold: Z. Physik **129** (1951) 123.
5) K. H. Paetzold and H. Krömer: Naturwiss. **5** (1953) 163.
6) I. Tsujikawa and S. Sugano: J. Phys. Soc. Japan **13** (1958) 220.